Hybrid composite based on conducting polymers and plasmonic nanomaterials applied to catalysis and sensing

To cite this article: Ahmed T Alanazi and James H Rice 2022 *Mater. Res. Express* **9** 075002

Materials Research Express

PAPER

Hybrid composite based on conducting polymers and plasmonic nanomaterials applied to catalysis and sensing

Ahmed T Alanazi and James H Rice*

School of Physics, University College Dublin, Belfield, Dublin 4, Ireland

* Author to whom any correspondence should be addressed.

E-mail: ahmed.alanazi@ucdconnect.i.e and james.rice@ucd.i.e

Keywords: catalysis, polymer, SERS, raman single, semiconductors, organic semiconductors

Supplementary material for this article is available online

OPEN ACCESS

RECEIVED
1 April 2022

REVISED
10 June 2022

ACCEPTED FOR PUBLICATION
30 June 2022

PUBLISHED
12 July 2022

Abstract

Combining plasmonic and semiconductors offers significant potential in creating sensing and photocatalytic devices. Nanocomposites including both metals and semiconductors can control the charge states in the metals that can enhance catalysis activity along with plasmon-enhanced spectroscopy. Here we demonstrate the use of conducting polymer materials with plasmonic nanomaterials to boost up to five-fold plasmon-enhanced Raman scattering spectroscopy signal strength and support oxidation of target molecules through supporting charge transfer processes. This work demonstrates the use of conducting polymers as a semiconductor platform to support plasmonic catalysis and sensing.

Introduction

Vibrational spectroscopy is a widely used method to characterize materials. One frequently used vibrational spectroscopy method is Raman scattering [1–4]. In Raman spectroscopy, only approximately one in 10^6 photons converted into stokes scattering light producing a weak analytical signal intensity [5–10]. However, the use of nanostructured materials can increase the efficiency of Raman scattering through plasmonic enhancement to enable single-molecule Raman detection [11, 12]. Modern material processing and characterization methods can produce nanomaterials, including metal nanostructures with a range of different geometries and properties [10, 13–16]. Localized surface plasmon resonance (LSPR) excitation results in a strongly enhanced electromagnetic field on the surface of the metal nanostructure [17, 18]. In addition to the electromagnetic-based mechanism to enhance Raman scattering, there is a chemical mechanism [19]. The chemical mechanism is less studied due to its relatively low Raman enhancement factors, in comparison to those of electromagnetic nature. The chemical mechanism can be assigned to arise from charge transfer processes such as those due to vibronic coupling of resonances in the molecule-substrate system providing Raman scattering signal enhancements [20–23].

Studies have shown that surface enhancement of Raman scattering (SERS) can be achieved through incorporating photo-induced surface oxygen vacancy states on semiconductors such as TiO_2 surfaces [24]. It was reported that the oxygen vacancy defects facilitated semiconductor-defect-metal-analyte vibronic couplings, furthering the Raman enhancement. The process was termed Photo-induced enhanced Raman Spectroscopy or simply PIERS [25–27]. PIERS trace level detection on a range of semiconductors [28] has been reported. In addition, to providing PIERS-based processes semiconductors can produce metal-semiconductor junctions that enable effective carrier separation through the formation of a Schottky junction [26, 29–31]. This junction is formed when the metal and semiconductor are in intimate contact, where the electrons from either semiconductor or metal migrate toward the other component to equilibrate their Fermi levels [23, 32–34]. A widely used conducting organic semiconductor is a blend of p and n-type semiconductors e.g. P3HT: PCBM. The polymer P3HT (poly 3 hexylthiophene) performs as an electron donor during the photo-excitation process and presents high charge mobility in well-crystallized film [35–37]. PCBM (phenyl C_{61}-butyric acid methyl

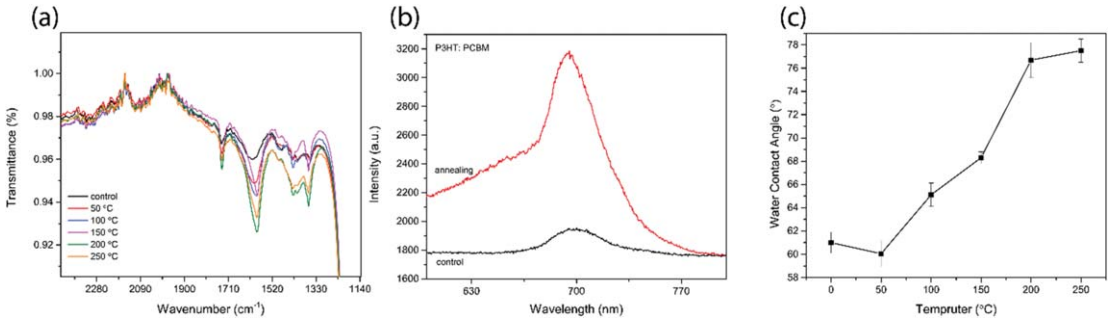

Figure 1. (a) FTIR spectra of the treated and nontreated P3HT: PCBM also showed different temperatures of 50, 100, 150, 200, and 250 °C in the oven for 40 min (b) fluorescence spectra of P3HT: PCBM before and after thermal annealing at 250 °C. (c) The water contact angle of the blended P3HT: PCBM shows different temperatures of 0 to 250 °C.

ester) acts as a matching candidate that will enable exciton dissociation to occur.[31, 32]. This polymer blend forms a Shockey junction with gold or silver (nanoparticles) [35, 38]. In this study, we combine P3HT: PCBM with silver nanoparticles (Ag NPs) as a platform to enhance Raman scattering. We demonstrate that this semiconductor-plasmonic system following thermal annealing enables a c.a.3-fold enhancement in SERS signal to be generated from analytes. Additionally, we show that the polymer supports plasmonic catalysis-based processes.

Results and discussion

P3HT:PCBM polymer blend was first prepared as a film and then thermally annealed (as outlined in supplicatory information). Thermal annealing has been shown to enhance the blending of the polymer enhancing charge transport efficiency [39]. The FTIR (fast transform infrared transmission) spectra of P3HT: PCBM blend prior to and following heat treatment, it is shown in (figure 1(a)). The FTIR spectrum of the polymer blend shows spectral features in line with literature reports [36, 40, 41]. Two clustered peaks appeared in the range of 2857–2958 cm^{-1} attributed to the presence of C–H band symmetric and asymmetric vibrations. The spectrum appears around 1500–1600 cm^{-1} showing the formation of C = C symmetric vibrations [36, 40, 41]. Following heat treatment the spectrum appears around 1600 cm^{-1} and 1400 cm^{-1} a slight peak shift to the right has been observed. A peak was also detected between 2750 to 3000 cm^{-1} after heat treatment (supplementary information figure 1). This is in line with literature studies indicating a morphology change in the polymer after thermal annealing [39].

The photoluminescence (PL) emission spectrum of the P3HT: PCBM blend (figure 1(b)) showed the expected broadband feature centred at c.a. 695 nm. Following annealing the polymer P3HT: PCBM at 250 °C for 40 min causes the PL emission band to become more intense. It has been reported that the degree of PL signal enhancement increases for thermally annealed films [40] an increase in PL signal intensity provides direct evidence for enhanced exciton recombination [40]. This enhanced exciton recombination yield within the P3HT:PCBM heterojunction occurs due to an increased separation between P3HT and PCBM [40, 42, 43]. Significantly this annealing also produces improvements in photovoltaic device efficiency associated with improved charge mobility, as compared to the un-annealed P3HT:PCBM polymer [42, 43]. The explanation for such improved photovoltaic device performance using annealed P3HT:PCBM blended polymer materials is through better charge mobility from increased polymer crystallization [42, 43]. Where P3HT and PCBM move from the amorphous to crystalline phase improving charge mobility following annealing. Femtosecond [44] time-resolved fluorescence studies of P3HT/PCBM blend films reported that thermal annealing of the polymer blend produced an increased contribution to PL of self-trapped dynamic localized excitons, which were competitive processes due to increased crystallization in the P3HT/PCBM blend film. This study [44] also reported a blue shift in the fluorescence for the annealed polymer blend which is in line with our studies (figure 1(b)) which also shows a blue shift of c.a. 10 nm for the annealed P3HT:PCBM blend.

Contact angle (CA) measurements were performed on the samples before and after annealed treatment 0, 50, 100, 150, 200, and 250 °C for 40 min in the oven. The average of 5 different spots on the sample was reported. The results indicate a considerable reduce in hydrophilicity of the surface as shown in (figure 1(c)) with the contact angle changed from 60 °C to 80 °C. Wettability of the surface is a recognised factor affecting the Raman signal intensity of a probe molecule deposited on it. Hydrophilic surfaces such as P3HT: PCBM organic semiconductors at a room temperature cause random spreading of analyte molecules while more hydrophobic surfaces contain a deposited drop to a small area and allow the droplets to keep their spherical shape during

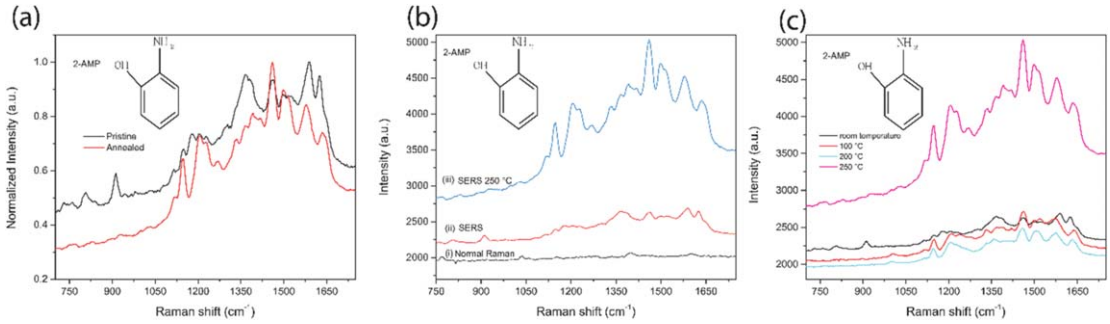

Figure 2. SERS measurements of aminophenol (2-AMP) recorded on the AgNP/P3HT: PCBM hybrid substrate (a) SERS spectra of thermally annealed (250 °C) and pristine P3HT: PCBM polymer blends with AgNPs and 2-AMP. (b) Normal Raman (black) Prior (red) following (blue) heat treatment. (c) A series of SERS spectra recorded for different annealing temperatures.

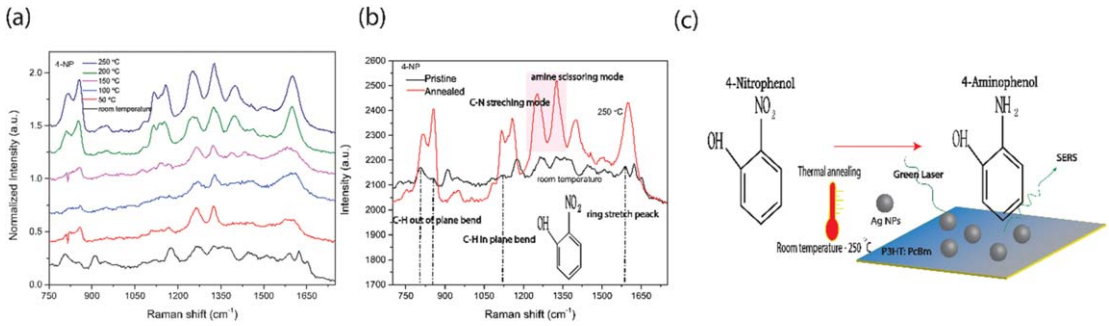

Figure 3. SERS spectra of 4-nitrophenol (4NP) recorded on P3HT: PCBM (a) SERS recorded on polymer blends that were annealed at different temperatures. (b) normalized SERS intensity prior (black) following (red) heat treatment. (c) Schematic of the oxidation reaction and formation of 4-aminophenol from 4-Nitrophenol.

solvent evaporation, resulting in an increase of the probe molecule concentration. A previous study shows an increase in the contact angles of the P3HT: PCBM blends with the annealing time at >150 °C [45] which makes the substrate hydrophobic and lowered the spot diameter of the deposited analyte.

We then studied the impact of thermal annealing the P3HT: PCBM/Ag NPs composite on the SERS signal intensity of 2-amino thiophenol (2-AMP) (figure 2). The 2-AMP SERS spectra [29] are described by peaks located at 1580, 1440, 1390, 1180, 1145, and 1098 cm^{-1}. These peaks are distinct from Raman peaks arising from the polymer blend (supplementary information figure 2). Comparing the SERS signal from the probe molecule on the thermally annealed substrate (treated at 250 °C) to the un-annealed substrate shows an increase in SERS signal intensity. The SERS signal recorded for the 250 °C annealed substrate shows a c.a. 5-fold increase in Raman signal (peak-to-peak) and a c.a. 2-fold increase in overall SERS signal intensity compared to when the polymer blend is unannealed. Inspection of the SERS spectra shows clear changes when comparing the SERS spectrum of 2-AMP on the un-annealed and 250 °C annealed substrate (figures 2(a)–(c)). The changes in the SERS spectra are assigned to a redox reaction, where 2-AMP is oxidized to 2-nitrophenol (2-NIP). Following heat treatment, 2-AMP has undergone a redox reaction, with the molecule 2-NIP formed from 2-AMP. The 2-NIP SERS [41–44] spectra is described by peaks located at 1617 cm^{-1} and 1590 cm^{-1}, 1536 cm^{-1}, 1472 cm^{-1}, 1326 cm^{-1} and 820 cm^{-1}. As the annealing temperature increases from room temperature to 250 °C the formation of 2-NIP increases (figure 2(c)). With Raman bands associated with 2-NIP becoming more visible with increasing annealing temperature.

We investigated if other probe molecule SERS signals could be boosted through thermal annealing of the substrate. The SERS spectra of 4-nitrophenol (4-NP) on the thermally annealed polymer blend (with AgNPs) were recorded (figure 3). The SERS spectra for the thermally annealed substrate at 250 °C showed a c.a. 5-fold increase in SERS signal (peak to peak ratio) compared to using the unannealed substrate. The SERS spectra recorded on this annealed substrate show SERS peaks at 1285 (C–N stretching mode) and 1334 (amine scissoring mode) cm^{-1} which signifies the transformation from 4-nitrophenol to 4-aminophenol [22].

The SERS signal from the probe molecule MB (methylene blue) was recorded (figure 4). Inspection of the SERS spectra shows that using the thermally annealed substrate (annealed at 250 °C) shows a c.a. 3-fold increase in SERS peak-to-peak signal intensity. The SERS spectra for MB showing characteristic ν(C−C) ring stretches at

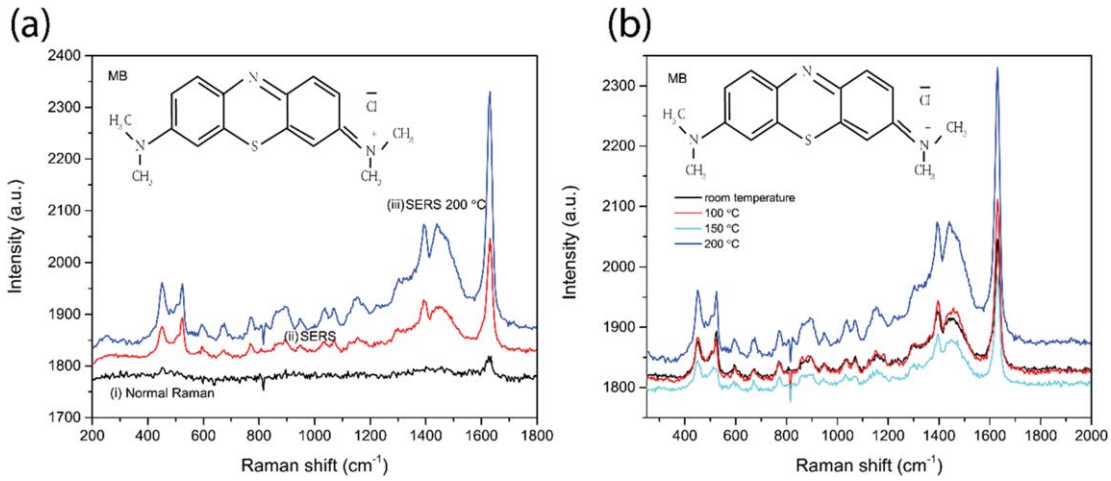

Figure 4. SERS measurements of MB were recorded on the Ag NPs/P3HT: PCBM hybrid substrate. (a) Normal Raman (black) SERS spectra were recorded prior (red) and following (blue) heat treatment. (b) The spectra show four different SERS spectra, corresponding to different annealing temperatures.

1621 cm^{-1}, ν(C−N) symmetric and asymmetric stretches at 1433 cm^{-1}, and δ(C−N−C) skeletal deformation mode at 450 cm^{-1} is observed which is in good agreement with the literature [46]. No changes in the SERS spectral features were observed other than changes in SERS signal intensity.

This increase in SERS signal for 2-AMP, 4NP and MB probe molecules, when recorded on the annealed 250 °C substrate, may be assigned to changes in surface wettability (figure 1(c)). However, thermal annealing of the substrate is shown to affect plasmonic catalysis activity (figures 2 and 3) implying that annealing the substrate may create changes to the electronic properties of the hybrid substrate that facilitates oxidation of 2-AMP to 2-NIP or 4-aminophenol from 4-Nitrophenol (figures 2 and 3 and supplementary information figure 3).

The energy levels shown in a band diagram for P3HT's conduction (CBM) and valance (VBM) band edges are 3.3 eV and 5.2 eV below the vacuum level respectively [37, 47]. The CBM and VBM energy levels for PCBM are located at 4.2 eV and 6.0 eV respectively [36]. The optical band gap value of P3HT is 1.9 eV and PCBM is 1.8 eV which allows for absorption of the Raman excitation lasers photons (2.3 eV). Following absorbing photons, excitons are generated in the polymer blend. For some of these excitons; electrons and holes are recombined; for other excitons, electrons and holes are separated and become free. Then free electrons move from P3HT to PCBM and free holes move from PCBM to P3HT shown in figure 5. The electrons then move to Ag NPs and then to the probe molecules resulting in increased SERS and catalysis activity [48]. Thermal annealing of the substrate enhances this process through more efficient charge mobility resulting in higher SERS signals and higher plasmonic catalysis activity.

Conclusion

We demonstrate the use of conducting polymer materials with plasmonic to boost plasmon-enhanced Raman scattering spectroscopy signal strength ($\leqslant$ 5-fold) and also support oxidation of target molecules on plasmon active nanostructures through assisting in charge transport-based processes. This charge-based process also enhances Raman scattering signals through an enhanced chemical mechanism. This work demonstrates the use of conducting polymers as semiconductor platforms to support plasmonic catalysis and sensing.

Materials and methods

Substrates and chemicals

All chemicals provided by sigma-Aldrich and frontier scientific the conducting polymers powder of Poly(3-hexythiophnene-2.5-dily) regioregular (P_3HT, CAS Number 104934–50–1) and [6,6]-Phenyl C_{61} butyric acid methyl ester ([60]PCBM, CAS Number 160848–22–6) were dissolved in chloroform ($ChCl_3$) to make 0.1 wt/vol % solution and sonicated for 30 min by means of ultra-sonic cleaning tank, aim of ensuring a uniform distribution in the diluent. The solution where then concentrated with chloroform ($ChCl_3$) to final concentration of 10^{-3} wt/vol %. The blend of P_3HT and PcBm was achieved by adding 500 μl of both solutions together 1:1 ratio. The thin film was made by drop deposition of 30 μl from the blend P_3HT:PcBM onto into a glass or silicon (Si-Mat, Thickness: 525 +/− 5 um) substrates. Then the solution lifted out at the room

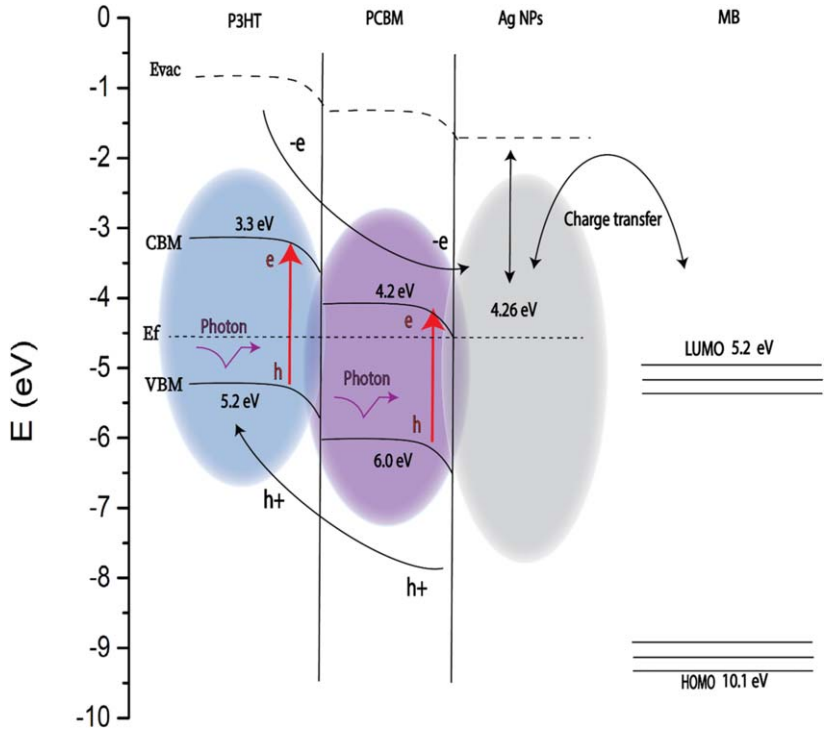

Figure 5. An energy band diagram illustrating the electronic transition between P3HT: PCBM and Ag NPs and the MB analyte molecule. The red lines show electron transitions excited by the Raman excitation laser.

temperature for 24 h to ensure it completely dry, then the samples were heated for 40 min in the oven at different temperatures 50, 100, 150, 200, 250 °C. After the annealed treatment we drop-cast 30 μl Ag NPS solutions (40 nm particle size) to be 1:1 ratio semiconductors to metals and lifted out at room temperature for 24 h no drying methods were used.

Preparation of probe molecule solutions

2-amino thiophenol (2-AMP), Methylene blue (MB) and 4-nitrophenol (4-NP) solution were prepared in methanol diluent at an former concentration of 10^{-2} M. The solution were then diluted with deionized water to a final concentration of 10^{-5} M. Then 30 μl of the probe molecule liquid was drop cast on the made substrates before the Raman measurements. 1:1:1: ratio (semiconductors: metals: Molecule).

Raman spectroscopy

SERS spectra were collected using 532 (nm) excitation wavelengths laser Power and energy meter: with microscopy slid power meter sensor head (SN: 09113026, S121 C, 400–1100 (nm), 500 (mW), LMR1/M, Thorlabs) and energy meter was used to measure the incident laser power. The energy of the laser power was focused by an attenuator at 5 mW in order to control the laser power at a distance of c.a. 8.2 mm for the entire experiment. Briefly, the beam pass through an interference filter and directed by mirror to angle prism which drives the beam at 90 towered the sample. Then, pass through lens which can be focusses onto the samples in order to have best signals, here the sample is excited and scattered light which is collected by lens and then pass through notch filter which is lowers the impact from the laser line before entries the spectrograph. Raman spectra were collected with an exposure time of 1 s and 10 accumulation mode . Calibration of the Raman spectrographic windows by acquiring a Raman spectrum from toluene and using it as a standard spectrum. the mean and standard deviation of 10 measurements is recorded.

Optical spectroscopy UV–vis absorption

Optical absorbance measurements of P3HT, PcBm, and P3HT/PcBm Concentration of 1×10^{-3} wt/vol % with and without Ag NPs. Measurements were achieved using an absorbance spectrometer (V-650, JASCO, Inc.)

as following settings, 1 nm step size, UV/Vis bandwidth of 2 nm, and 200 nm/min scan speed through a 200–800 nm range. A coverslip substrate was employed to accomplish the measurements.

Fourier transform infrared spectroscopy

Fourier transform infrared spectroscopy (FTIR) set up measurement parameter resolution 4 cm^{-1}, sample scan time 8 scans, measurement time $>$ 10 s, saved data from 400–4000 cm^{-1}, result spectrum transmission mode, accessory ATR platinum diamond. We have recorded FTIR spectrum of P3HT, PcBM, and the blend P3HT: PcBm as a solid state. FTIR instrument have been collected by using Alpha Platinum Bruker system.

Contact angle

A contact angle has been applied to determent surface Chemistry of the conducting polymers at different temperatures starting with room temperature, 50, 100, 150, 200, 250 °C by using (Kruss Advance Drop Shape Analyser DSA25E). A deionized water droplet on treat and untreated substrates has been added to the surface and then the average of c.a. 5 measurements is taken.

Scanning electron microscopy

High-resolution scanning electron microscopy (SEM) images were obtained using a Sigma 300 gemini scanning electron microscopy system. Control panel status scanning operation mode normal scan speed 8 cycle time 1 min zoom factor 2.

Associated content supporting information

Figures S1—S8 (available online at stacks.iop.org/MRX/9/075002/mmedia) - Further data related to SERS spectra have been used for the purpose of identify the peaks of the organic semiconductors spectra, measurement of substrate stability and reproducibility. High-resolution scanning electron microscopy (SEM), Atomic Force Microscopy (AFM) images, Optical spectroscopy UV–vis absorption.

Acknowledgments

We acknowledge the Saudi Arabian government scholarship program for supporting this work, the Ministry of Education–Kingdom of Saudi Arabia (MOE, Ref. No. IR18131), and the Saudi Arabian Cultural Mission (SACM, Grant No. 01102019). The authors acknowledge for Denis Dowling and Andrew Dickson assistance with contact angle measurements. The authors also acknowledge for Gareth Redmond for access to UV–vis spectroscopy; Aaron Martin and Hans Eckhardt for access to FTIR spectroscopy; and Brian Rodriguez for access to AFM, the oven, and UV-Ozone.

Data availability statement

All data that support the findings of this study are included within the article (and any supplementary files).

Author contributions

A.T.A and J.H.R. constructed the experiments and established the experimental process. A.T.A performed the sample preparation, SEM, Raman, and fluorescence measurements. A.T.A fulfil UV–vis, FTIR, contact angle, XPS measurements. All authors evaluated data, reviewed results, and wrote the manuscript. All authors have given approval to final version of the manuscript.

Funding

This publication has arisen from research organized with the Saudi Arabian government scholarship program, the Ministry of Education–Kingdom of Saudi Arabia (MOE, Ref. No. IR18131), and the Saudi Arabian Cultural Mission (SACM, Grant No. IR18131).

Notes

The authors declare no competing financial interest.

ORCID iDs

Ahmed T Alanazi https://orcid.org/0000-0002-8381-1815
James H Rice https://orcid.org/0000-0002-1035-5708

References

[1] Lordan F, Rice J H, Jose B, Forster R J and Keyes T E 2011 Site selective surface enhanced Raman on nanostructured cavities *Appl. Phys. Lett.* **99**
[2] Damm S *et al* 2014 Application of AAO matrix in aligned gold nanorod array substrates for surface-enhanced fluorescence and raman scattering *Plasmonics* **9** 1371–6
[3] Al-Attar N *et al* 2012 Surface-enhanced raman scattering from small numbers of purified and oxidised single-walled carbon nanotubes *Chem. Phys. Lett.* **535** 146–51
[4] McNamara D *et al* 2015 A raman spectroscopy investigation into the influence of thermal treatments on the residual stress of polycrystalline diamond *Int. J. Refract. Met. Hard Mater.* **52** 114–22
[5] Almohammed S, Zhang F, Rodriguez B J and Rice J H 2019 Electric field-induced chemical surface-enhanced raman spectroscopy enhancement from aligned peptide nanotube-graphene oxide templates for universal trace detection of biomolecules *J. Phys. Chem. Lett.* **10** 1878–87
[6] Almohammed S, Fedele S, Rodriguez B J and Rice J H 2017 Aligned diphenylalanine nanotube–silver nanoparticle templates for high-sensitivity surface-enhanced Raman scattering *J. Raman Spectrosc.* **48** 1799–807
[7] Alattar N *et al* 2018 Surface-enhanced Raman scattering for rapid hematopoietic stem cell differentiation analysis *Appl. Opt.* **57** E184
[8] Al-Shammari R M *et al* 2018 Photoinduced enhanced raman from lithium niobate on insulator template *ACS Appl. Mater. Interfaces* **10** 30871–8
[9] Fularz A, Almohammed S and Rice J H 2021 SERS enhancement of porphyrin-type molecules on metal-free cellulose-based substrates *ACS Sustain. Chem. Eng.* **9** 16808–19
[10] Alanazi A T, Almohammed S and Rice J H 2022 Plasmonic photo-catalysis using a CdS–silver nanowire composite, *AIP Adv.* **12** 025223
[11] Sharma B, Frontiera R R, Henry A I, Ringe E and Van Duyne R P 2012 SERS: materials, applications, and the future. *Mater. Today* **15** 16–25
[12] Al-Shammari R M *et al* 2018 Single-molecule nonresonant wide-field surface-enhanced raman scattering from ferroelectrically defined Au nanoparticle microarrays *ACS Omega* **3** 3165–72
[13] Rice J H *et al* 2005 Biexciton and exciton dynamics in single InGaN quantum dots *Nanotechnology* **16** 1477–81
[14] Kennedy E, Al-Majmaie R, Al-Rubeai M, Zerulla D and Rice J H 2013 Nanoscale infrared absorption imaging permits non-destructive intracellular photosensitizer localization for subcellular uptake analysis *RSC Adv.* **3** 13789–95
[15] Schwell M *et al* 2001 Coupling a dendrimer and a fullerene chromophore: a study of excited state properties of C61 (poly(aryl) acetylene) 2 *Chem. Phys. Lett.* **339** 29–35
[16] Almohammed S *et al* 2016 Wettability gradient-induced alignment of peptide nanotubes as templates for biosensing applications *RSC Adv.* **6** 41809–15
[17] Damm S *et al* 2015 Plasmon enhanced fluorescence studies from aligned gold nanorod arrays modified with SiO_2 spacer layers *Appl. Phys. Lett.* **106** 183109
[18] Lordan F *et al* 2013 The effect of Ag nanoparticles on surface-enhanced luminescence from Au nanovoid arrays *Plasmonics* **8** 1567–75
[19] Ryan K *et al* 2017 Thermal and aqueous stability improvement of graphene oxide enhanced diphenylalanine nanocomposites *Sci. Technol. Adv. Mater.* **18** 172–9
[20] Seo J *et al* 2020 Ultrasensitive plasmon-free surface-enhanced raman spectroscopy with femtomolar detection limit from 2D van der waals heterostructure *Nano Lett.* **20** 1620–30
[21] Sun S and Wu P 2011 Competitive surface-enhanced Raman scattering effects in noble metal nanoparticle-decorated graphene sheets *Phys. Chem. Chem. Phys.* **13** 21116–20
[22] Zheng Z *et al* 2017 Semiconductor SERS enhancement enabled by oxygen incorporation *Nat. Commun.* **8** 2–11
[23] Rice J H *et al* 2004 InGaN quantum dots grown by MOVPE via a droplet epitaxy route. *Phys. E Low-Dimensional Syst. Nanostructures* **21** 546–50
[24] Glass D *et al* 2019 Dynamics of photo-induced surface oxygen vacancies in metal-oxide semiconductors studied under ambient conditions *Adv. Sci.* **1901841** 1901841
[25] Fularz A, Almohammed S and Rice J H 2020 Oxygen incorporation-induced SERS enhancement in silver nanoparticle-decorated ZnO nanowires *ACS Appl. Nano Mater.* **3** 1666–73
[26] Rice J H, Fularz A and Almohammed S 2020 Controlling plasmon-induced photocatalytic redox reactions on WO_3 nanowire/AgNPs substrates via defect engineering *J. Phys. Chem. C* **124** 25351–60
[27] Zhao J *et al* 2021 Recent advances and perspectives in photo-induced enhanced Raman spectroscopy *Nanoscale* **13** 8707–21
[28] Ben-Jaber S *et al* 2016 Photo-induced enhanced Raman spectroscopy for universal ultra-trace detection of explosives, pollutants and biomolecules *Nat. Commun.* **7** 1–6
[29] Almohammed S, Barwich T, Mitchell S, Rodriguez A K and Rice J H 2019 Enhanced photocatalysis and biomolecular sensing with field-activated nanotube-nanoparticle templates *Nat. Commun.* **10** 1–11
[30] Almohammed S *et al* 2020 Flexing piezoelectric diphenylalanine-plasmonic metal nanocomposites to increase SERS signal strength *ACS Appl. Mater. Interfaces* **12** 48874–81
[31] Lordan F *et al* 2013 Temperature dependence of a1 and b2 type modes in the surface enhanced raman from 4-aminobenzenethiol *Chem. Phys. Lett.* **556** 158–62
[32] Rice J H, Galaup J P and Leach S 2002 Fluorescence and phosphorescence spectroscopy of C70 in toluene at 5 K: Site dependent low lying excited states *Chem. Phys.* **279** 23–41

[33] Fedele S, Hakami M, Murphy A, Pollard R and Rice J 2016 Strong coupling in molecular exciton-plasmon Au nanorod array systems *Appl. Phys. Lett.* **108** 053102
[34] Ferdele S, Jose B, Foster R, Keyes T E and Rice J H 2017 Strong coupling in porphyrin J-aggregate excitons and plasmons in nano-void arrays *Opt. Mater. (Amst).* **72** 680–4
[35] Fanti M *et al* 2002 C70Ph8 and C70Ph10: a computational and solid solution spectroscopic study *J. Chem. Phys.* **116** 7621–6
[36] Arulraj A, Bhuvaneshwari S, Senguttuvan G and Ramesh M 2018 Solution processed inverted organic bulk heterojunction solar cells under ambient air-atmosphere *J. Inorg. Organomet. Polym. Mater.* **28** 1029–36
[37] Murali M G, Rao A D, Yadav S and Ramamurthy P C 2015 Narrow band gap conjugated polymer for improving the photovoltaic performance of p3ht:pcbm ternary blend bulk heterojunction solar cells *Polym. Chem.* **6** 962–72
[38] Kumar S *et al* 2018 Study of P3HT/ PCBM morphology using Raman spectroscopy *AIP Conf. Proc.* **1953** 1–5
[39] Jeong G, Choi S, Jang M and Chang M 2021 Thermal annealing effects on the morphology and charge transport of polymer semiconductor nanowires aligned in an insulating polymer matrix *Dye. Pigment.* **185** 108962
[40] Kalonga G 2013 Characterization and optimization of poly (3-hexylthiophene-2, 5- diyl) (P3HT) and [6, 6] phenyl-C61-butyric acid methyl ester (PCBM) blends for optical absorption *J. Chem. Eng. Mater. Sci.* **4** 93–102
[41] Ng A *et al* 2014 P3HT: PCBM solar cells - the choice of source material *J. Appl. Polym. Sci.* **131** 2
[42] Pearson A J *et al* 2012 Rationalizing phase transitions with thermal annealing temperatures for P3HT:PCBM organic photovoltaic devices *Macromolecules* **45** 1499–508
[43] Wang T, Pearson A J, Lidzey D G and Jones R A L 2011 Evolution of structure, optoelectronic properties, and device performance of polythiophene:fullerene solar cells during thermal annealing *Adv. Funct. Mater.* **21** 1383–90
[44] Xie Y *et al* 2010 Femtosecond time-resolved fluorescence study of P3HT/PCBM blend films *J. Phys. Chem. C* **114** 14590–600
[45] Karagiannidis P G, Georgiou D, Pitsalidis C, Laskarakis A and Logothetidis S 2011 Evolution of vertical phase separation in P3HT: PCBM thin films induced by thermal annealing *Mater. Chem. Phys.* **129** 1207–13
[46] Rodríguez-Torres M, Del P, Díaz-Torres L A and Romero-Servin S 2014 Heparin assisted photochemical synthesis of gold nanoparticles and their performance as SERS substrates *Int. J. Mol. Sci.* **15** 19239–52
[47] Ansari M A, Mohiuddin S, Kandemirli F and Malik M I 2018 Synthesis and characterization of poly(3-hexylthiophene): Improvement of regioregularity and energy band gap *RSC Adv.* **8** 8319–28
[48] Whitcher T J *et al* 2014 Determination of energy levels at the interface between O2 plasma treated ITO/P3HT : PCBM and PEDOT : PSS/P3HT :PCBM using angular-resolved x-ray and ultraviolet photoelectron spectroscopy *J. Phys. D: Appl. Phys.* **47** 055109